Quantifying the Dependence of Battery Rate-Performance on Electrode Thickness

Dominik V. Horváth[1], João Coelho[2], Ruiyuan Tian,[1,*] Valeria Nicolosi[2] and Jonathan N. Coleman[1*]

[1]*School of Physics, CRANN & AMBER Research Centres, Trinity College Dublin, Dublin 2, Ireland*

[2]*School of Chemistry, CRANN & AMBER Research Centres, Trinity College Dublin, Dublin 2, Ireland*

*colemaj@tcd.ie, RTIAN@tcd.ie

ABSTRACT: Simultaneous optimisation of capacity and rate-performance in battery electrodes would be much simplified by access to a simple equation relating rate-performance to electrode thickness. While a number of equations have been proposed, data on the effect of electrode thickness on rate-performance is not extensive enough to identify the most appropriate model for thickness-dependence. Here, using $LiNi_{0.815}Co_{0.15}Al_{0.035}O_2$ (NCA) as a model system, we use chronoamperometry as a procedure to rapidly generate capacity-rate curves for >50 different electrode thicknesses. Using a semi-empirical fitting equation, we extract the characteristic time (τ) associated with charge/discharge for each thickness (L_E). We find the resultant τ-L_E curve to be inconsistent with minimal models based on liquid- or solid-phase-diffusion alone, but to be in excellent agreement with a relatively simple rate model which includes liquid- and solid-phase-diffusion effects as well as electrical and electrochemical limitations. Thickness-dependent impedance measurements show that the magnitudes of the electrochemical and solid-state diffusion contributions are perfectly in line with the outputs of the rate model.

INTRODUCTION

The demand for efficient energy storage solutions is expected to remain high as the world expands the use of electric vehicles. Rechargeable Li-ion batteries (LIBs) are used to satisfy much of this demand thanks to their efficiency, cyclability and high capacity.[1] While maximisation of capacity and energy density is the focus of many papers on LIBs, achieving good rate-performance is also important, both for high power and fast-charging purposes, especially for applications in electric vehicles.[2]

However, combining good rate-performance with high absolute capacity can be challenging. The accessible capacity of a battery electrode can depend strongly on the current (i.e. rate) at which it is charged or discharged. While high capacities, even approaching the theoretical maximum, might be achieved at low charge/discharge currents, the achievable capacity tends to fall off sharply above some threshold charge/discharge current, I_T. For analysis purposes, it is often useful to consider the charge discharge rate, R, which we define rate as charge/discharge current divided by measured capacity at that current: $R=I/Q$.[3,4] Then the threshold rate, above which capacity falls off is given by $R_T=I_T/Q$. Clearly, we would want this threshold rate to be high in order to achieve maximal capacity at as high a rate as possible. However, various papers have shown that R_T depends strongly on a number of electrode parameters including conductivity, porosity and thickness.[3,5-8]

In particular, the dependence of battery properties on electrode thickness is a very significant (and often neglected) area because of the opposite dependences of capacity and rate-performance on thickness. Increasing electrode thickness enhances areal capacity and is an accepted strategy to improve energy density.[6] However, as mentioned above, increasing thickness also results in a reduction in R_T and hence a degradation of rate-performance.[3,5,9,10] The combination of these effects means that while thin electrodes display low absolute capacity but excellent rate-performance, thick electrodes display high absolute capacity only at low rate. As a result there is a trade-off between maximisation of capacity and rate-performance[4] that is not always fully appreciated.

One way to optimise the trade-off between capacity and rate-performance, is to identify the electrode thickness where the best combination of these parameters occurs.[4] To do this, it is important to understand in quantitative detail how both capacity and rate-performance scale with electrode thickness. If both scalings are known, it is straightforward to develop an

equation which yields the optimum electrode thickness in terms of the physical parameters of the system.[4] For capacity, there is a simple relationship between areal capacity (*Q/A*) and thickness (L_E): $Q/A = L_E \times Q/V$ where *Q/V* is the volumetric capacity. However, the situation is not so simple for rate-performance. Firstly, one must identify a quantitative figure of merit for rate-performance. Secondly, the dependence of that figure of merit on electrode thickness must be well known. While there are candidates for use as figures of merit and proposals for their length dependence (see below), a final candidate has not been agreed upon.

Usually, rate-performance is reported by quoting specific capacities at high specific currents.[11] However, this approach can be misleading as it ignores electrode thickness (while a high specific capacity may be demonstrated at high specific current using very thin electrodes, this will not be achievable using electrodes of thickness relevant to practical applications).[12,13] Preferably, a figure of merit for rate-performance should be a single number which can be measured in a reproducible way and can be quantitatively related to electrode properties through a physical model. One candidate for such a figure of merit would be the threshold rate, above which capacity begins to decay (R_T).[10,14,15] Alternatively, the inverse of R_T can be related[4,16] to a characteristic time, τ, which is a measure of the minimum charge/discharge time which still yields the maximal capacity.[3,4,7,8,11,17] Recently, we proposed a semi-empirical equation[3,8] which can be used to fit capacity-rate data outputting τ in a reproducible manner. We have demonstrated that this parameter is a powerful figure of merit which can be used to quantify the dependence of rate-performance on a number of factors such as electrode thickness, conductivity and porosity as well as ion diffusivity and ionic conductivity.[3,11,18]

This leaves the question as to how exactly τ depends on electrode thickness. A number of papers have proposed models which can be used to generate equations for τ in terms of electrode thickness.[16] For example, both Cornut et al. and Wong et al. have proposed models based on solid state diffusion which would imply that τ does not depend on L_E at all (i.e. $\tau \propto L_E^0$).[15,19] Perhaps more relevant, Heubner et al.[7,10,14] have published a set of papers based on liquid phase diffusion limitations which either explicitly or implicitly[16] propose that $\tau \propto L_E^2$. Similarly, both Johns et al.[20] and Gallagher et al.[21] proposed diffusion limited models which can be modified[16] to give the same result. However, all of these models focus on single rate limiting effects. In reality, multiple factors may simultaneously affect rate-performance. Recently, we proposed a model for τ which incorporated a number of rate limiting effects

including diffusive and capacitive (electrical) and electrochemical factors.[3] This paper proposed an equation for τ in terms of L_E with included quadratic ($\propto L_E^2$), linear ($\propto L_E$) and constant ($\propto L_E^0$) terms. Fitting of a number of published data sets showed very good agreement and implied that a single quadratic term ($\tau \propto L_E^2$) is not enough to describe most experimental data.

However, this outcome cannot be considered conclusive, simply because published electrode thickness dependent capacity-rate data sets are not extensive enough. Published papers tend to report capacity *versus* rate curves (which can be fitted to get τ) for no more than 4-6 electrode thicknesses. This is simply not enough data to definitively prove one model over another. The reason for the lack of published data is simple. Galvanostatic charge discharge (GCD) measurements, which are normally used to characterise rate-performance, can be extremely slow, especially at low rate (low current). This limits the number of capacity-rate data points that can practically be measured in a given study with the outcome being: either a limited number of capacity-rate data points in each capacity *versus* rate curve, and/or a small number of capacity *versus* rate curves in a given study. Such limitations make it prohibitive to acquire the type of large data sets needed to test models. However, this paradigm has recently changed with the demonstration by Heubner et al.[22] (and confirmation by us[8]) that chronoamperometry (CA) can be used to obtain extensive capacity-rate data sets in a much more rapid fashion. CA allows individual capacity *versus* rate curves to be measured at least ×3 times faster than using GCD. This capability allows the generation of the type of extensive data sets, consisting of multiple capacity *versus* rate curves, required to test models for rate-performance. In addition, a capacity *versus* rate data set obtained by CA might have thousands of data points, orders of magnitude more than GCD-based capacity *versus* rate curves that typically contain <10 data points. Recently, we have used this capability to quantitatively analyse the dependence of τ on electrode conductivity.[18]

In this paper, we characterise the rate-performance of a model electrode system at a wide range of thicknesses (10-257 μm) using CA to record capacity-rate data. We employ the semi-empirical fitting equation proposed by Tian et al.[3] to obtain τ and analyse its dependence on electrode thicknesses. This work clearly shows that a single quadratic term ($\tau \propto L_E^2$) cannot describe our data but, at the very least, a linear term ($\propto L_E$) must be added, with the likelihood

that a small constant ($\propto L_E^0$) term is also needed. By fitting the data to our previously proposed model, we show that the model fit parameters are quantitatively consistent with expectations. Furthermore, we use electrochemical impedance spectroscopy (EIS) to analyse the thickness dependent capacitive, diffusive and charge-transfer properties of the electrodes, obtaining results which support the outputs of our rate model.

RESULTS AND DISCUSSION

Electrode materials

In order to quantitatively study the dependence of rate-performance on electrode thickness, we chose $LiNi_{0.815}Co_{0.15}Al_{0.035}O_2$ (NCA) as a model system due to its high usable discharge capacity, high specific energy and power density, and long storage cycle life.[23] In addition, we chose to use 0.5 wt% single-walled nanotubes (CNT) as both binder and conductive additive due to their proven record for yielding high specific capacities even at high electrode thickness.[6] Battery cathodes for electrochemical measurements were produced via slurry casting a mixture of CNT and NCA powder, as described in the methods section. The anodes were evaluated in a half-cell configuration with Li as the counter electrode. Two sets of cells were prepared, one with a separator thickness (L_S) of 16 μm and another with L_S = 38 μm. Both sets contained a wide range of electrode thicknesses, ranging from ~10 μm to ~250 μm.

The NCA electrode morphology was examined using scanning electron microscopy (SEM), with a typical cross-sectional image shown in figure 1A. This shows the electrode to consist of large (~10 μm), roughly spherical "secondary particles" of NCA with sections of the nanotube segregated network just visible (white arrows). We note that no significant changes in morphology were observed for electrodes of different thickness (Figure S1). Figure 1B shows a magnified image showing a number of secondary particles as well as a closer view of the nanotube network (white arrow). The NCA secondary particles are made up of agglomerates of primary particles as shown in figure 1C. This image also shows a number of nanotubes (e.g. as illustrated by the arrow) wrapping the secondary particle. Shown in Figure 1D is a histogram of the NCA primary particles' size (i.e. diameter) as measured by SEM. The primary particles have an average size of 645±24 nm, in agreement with literature (670 nm).[24] Similarly, a histogram of the secondary particles' diameter is shown in Figure 1E, with an average diameter

of 8.4±0.5 μm, close to the manufacturers specifications and in line with previous reports (~6 μm).[25]

Figure 1B shows how the CNTs assemble into a web-like structure around the NCA secondary particles. This is a segregated network, which occurs when the CNT network is forced to wrap around large particles.[6] These networks yield high electronic conductivity: here we measured the average out-of-plane conductivity of our electrodes to be 0.4 S/, surprisingly high for such a low CNT loading. In addition, such networks generate very high toughness which has been shown to facilitate the production of very thick electrodes.[6] Furthermore, the use of CNTs tends to give large low-rate capacities, which often approach the theoretical value.[6,26,27]

Rate measurements

To obtain rate-performance data, chronoamperometric current transients (see ref [8] for more information) were recorded for each electrode thickness over both sample sets. The current transient data was then converted[8] to specific capacity (*Q/M*) versus charge/discharge rate (*R*) as described in Methods. Here, *R* is defined as $R = (I / M) / (Q / M)$, where *I/M* is the specific current (current per unit mass) and *Q/M* is the experimental specific capacity measured at *I/M*, rather than the theoretical capacity, which is used to calculate C-rate. In this way, R^{-1} is a measure of the actual charge/discharge time (rather than some notional charge/discharge time that might only apply at low rate, as is the case with C-rate). This is important if one is to perform quantitative analysis.

Figure 2 plots *Q/M* vs. *R* for four representative values of L_E (see figure S2-4 for all data) We note that the data density is much higher than obtained from GCD measurements and data points are available even in the very low *R* regime. It is evident that the rate (R_T) at which *Q/M* starts to decline, shifts from high *R* to low *R* with increasing L_E. This is indicative of rate-performance getting worse for thicker electrodes, as has been qualitatively demonstrated previously.[3,5,28,29]

Before discussing the rate-performance, it is worth noting that the low-rate capacity, extracted from the rate curves for these electrodes at R=0.01 h^{-1}, is relatively high (referred to as $(Q/M)_{0.01\ 1/h}$). Shown in Figure 3A are values of $(Q/M)_{0.01\ 1/h}$ plotted versus electrode thickness, L_E, for NCA-NT composite electrodes measured using separators with two different thicknesses. We find that, for thin electrodes, the low-rate capacity is roughly thickness-independent at ~200 mAh/g, very close to the theoretical capacity of NCA (196 mAh/g). However, we do see a

slight fall off in $(Q/M)_{0.01\ 1/h}$ for thicknesses above ~100 μm, possibly indicating reduced electrolyte penetration into very thick electrodes. Averaging over all electrodes with thickness <100 μm gives an average value of $(Q/M)_{0.01\ 1/h}$=201 mAh/g.

Fitting capacity-rate data

We now focus on analysing the rate-performance. Recently,[3] we demonstrated a simple method for generating the characteristic time, τ, referred to above. We showed that rate-performance can be assessed by fitting capacity-rate data to a semi-empirical equation:

$$\frac{Q}{M} = Q_M\left[1-(R\tau)^n\left(1-e^{-(R\tau)^{-n}}\right)\right] \quad (1)$$

Here *Q/M* is the measured specific capacity (mAh/g, here normalised to active mass) while *R* is the rate defined via the specific current (*I/M*) as $R = (I/M)/(Q/M)$. We note that, unlike C-rate, which is defined via the theoretical capacity, *R* is calculated from the measured specific capacity (at a given current). In this way, *R* is a measure of the actual charge/discharge time. Fitting *Q/M* vs. *R* data yields the parameters Q_M, τ and *n*, of which the last two quantify the rate-performance. We note that the parameter, Q_M, represents the specific capacity at very low rate. For GCD measurements, the best way to reliably obtain this value is via fitting using equation (1). However, when using CA data, because very low values of *R* are available, the low-rate capacity can be reliably read of the graph (i.e. $(Q/M)_{0.01\ 1/h}$ as shown in Figure 3A).

As mentioned above, τ is the characteristic time associated with charge/discharge and can be considered the minimum time required to charge the electrode to its maximum capacity. This parameter is particularly useful as it can be related to R_T,[4,16] the threshold rate above which the capacity falls off. If we define R_T as the rate at which the capacity has fallen to 90% of its maximum, low rate value, then $R_T = (0.1)^{1/n}/\tau$ (see figure 2). Because of its relationship with R_T, which is an important physical parameter, τ is a useful figure of merit for rate-performance.

Finally, *n* describes how rapidly *Q/M* decays at high rate. Taylor-expanding the exponential in equation 1 (retaining the first three terms) shows the high-rate behaviour to be given by $(Q/M)_{highR} \approx Q_M(R\tau)^{-n}/2$. Thus, *n* is the exponent controlling the power-law decay of capacity with rate at high-rate (figure 2). Diffusion limited electrodes are thought to give *n*~0.5

while electrodes limited by electrical resistances yield n~1.[3] Knowledge of τ and n allow a proper quantitative analysis of the rate-performance of a given electrode and the comparison with other electrodes.

A number of papers[3,4] have shown equation (1) to fit capacity-rate data obtained from galvanostatic charge-discharge data extremely well. We have used this function to fit all capacity-rate data sets for NCA electrodes with different electrode and separator thicknesses with examples shown in Figure 2. In all cases the equation fits the capacity-rate curves extremely well at both high rates as well as intermediates rates (i.e. for R~R_T). However, we note that, for the thinner electrodes, the fit quality is not perfect at very low values of R, a factor that we attribute to the details of the CA response of NCA. In all cases, we extracted values of τ and n from the fits as will be discussed below.

To quantify rate-performance, the most important parameter is τ, which is plotted versus L_E in Figure 3B for both separator types (n-data will be discussed below). This graph shows τ to increase strongly with L_E: over an ×30 increase in electrode thickness we find a roughly ×250 increase in time constant (consistent with a significant reduction in rate-performance as L_E is increased). We note that such a degradation in rate-performance with increasing thickness has been reported by a number of researchers[5,29,30] with a number of such published data sets presented as τ *versus* R in our recent review paper.[3] The sample set with the thicker separator displays consistently higher values of τ over the whole L_E-range although this difference is most apparent for thinner electrodes.

In the past, graphs of τ *versus* L_E have usually included only 4-6 electrode thicknesses[3] which is not enough to definitively quantify the thickness dependence. Here, including both separator types, we have measured 51 different electrodes with thickness ranging between 10 and 250 μm. We believe such an extensive thickness-dependent study is unprecedented and will allow us to quantify the dependence of τ (and so the rate-performance) on L_E.

As discussed in the introduction, a number of papers have proposed that $\tau \propto L_E^2$, under the assumption that rate-performance is limited by diffusion of ions within the porous interior of the electrode.[7,10,14] If this were the case, then we would expect;[3] $\tau = L_E^2 / D_{BL} P_E^{3/2}$, where P_E is the porosity of the electrode and D_{BL} is the ion diffusion coefficient in the bulk electrolyte. We have plotted this prediction on figure 3C (dashed line) approximating[31,32] D_{BL}=3×10^{-10} m^2/s

and using P_E=0.31 (calculated from the electrode density of 3.1 g/cm^3). Although the dashed line is parallel to the experimental data for very thick electrodes, it is approximately ×8 below the experimental data. In addition, it is clear that the $\tau \propto L_E^2$ behaviour described by this minimal model cannot describe thin electrodes, which deviate significantly from the $\tau \propto L_E^2$ behaviour. Such a deviation is reasonable as thin electrodes might be expected to be limited by solid state diffusion in active particles, a behaviour which should be independent of L_E. In any case, this clearly shows that liquid-diffusion models proposing $\tau \propto L_E^2$ alone are not sufficient to describe rate-performance. Although this mechanism may be dominant under certain circumstances, in general, we expect a number of other processes such as electrical effects[18,33] or solid state diffusion[19,34] to also contribute to the rate limitations.

Quantitative analysis of τ data

Clearly the τ *versus* L_E behaviour is too complex to be described by models incorporating a single rate limiting process but actually depends on multiple processes occurring in concert. We can understand these results by considering a model which we recently reported, which describes τ in terms of the various timescales associated with electron and ion motion in the system.[3] There are three main contributions to τ: the RC charging time associated with the system, the timescale associated with ion diffusion and the time associated with the electrochemical reaction (see ref [3] for more information). Each of these contributions can be broken into one or more terms which can be combined to yield equation (2a). The RC terms include contributions from the electrical resistance of the electrode (term 1) as well as the ionic resistances of the electrolyte within the pores of the electrode (term 2) and within the separator (term 4). The diffusive terms include contributions from the times required for ions to diffuse through the electrolyte-filled porous interior of the electrode (term 3), the time required to diffuse through the separator (term 5) and the solid-state diffusion time (term 6). The final term (7) describes the timescale associated with the electrochemical reaction, t_c, which we link below to the exchange current density via the charge transfer resistance.

This yields the following equation[3]

$$\tau = L_E^2\left[\frac{C_{V,eff}}{2\sigma_{OOP}} + \frac{C_{V,eff}}{2\sigma_{BL}P_E^{3/2}} + \frac{1}{D_{BL}P_E^{3/2}}\right] + L_E\left[\frac{L_S C_{V,eff}}{\sigma_{BL}P_S^{3/2}}\right] + \left[\frac{L_S^2}{D_{BL}P_S^{3/2}} + \frac{L_{AM}^2}{D_{AM}} + t_c\right]$$

Term 1 2 3 4 5 6 7

(2a)

Here $C_{V,eff}$ is the effective volumetric *capacitance* of the electrode, σ_{OOP} is the out-of-plane[18] electronic conductivity of the electrode material, P_E and P_S are the porosities of the electrode and separator respectively while L_S is the separator thickness. Here σ_{BL} is the overall (anion and cation) ionic conductivity of the bulk electrolyte (S/m) while D_{BL} is the ion diffusion coefficient in the bulk electrolyte. In addition, L_{AM} is the solid-state diffusion length associated with the active particles (related to particle size); D_{AM} is the solid-state Li ion diffusion coefficient within the particle. It should be noted that D_{AM} is an effective value, averaged over all states of charge. In most cases, the volumetric capacitance of a battery electrode will not be known. However, we have shown empirically that $C_{V,eff}$ is directly proportional to the low-rate total (i.e. normalised to total electrode volume) volumetric capacitance of the electrode, Q_V, which applies over a range of electrode materials, such that $C_{V,eff} / Q_V = 28$ F/mAh appears to be a general relation.[3,18]

Equation (2a) is a trinomial quadratic equation which can be written in abbreviated form:

$$\tau = aL_E^2 + bL_E + c$$

(2b)

where *a*, *b* and *c* can be found by comparison of equations (2a) and (2b) (see below). This function clearly has the correct form to describe the data in Figure 3B as it will be dominated by the L_E^2 term at high electrode thickness but will be much flatter for thin electrodes as one or both of the other terms dominate. We have fitted equation (2b) to the data in Figure 3B for both separator thicknesses, finding very good fits in each case. The fit parameters are given in the panel (see figure caption for errors).

We can test the model by comparing the fit parameters to equation (2a). We start with the *b*-parameter. By comparison of equations (2a) and (2b):

$$b = L_S C_{V,eff} / \sigma_{BL} P_S^{3/2}$$

(3a)

Because the blue and red data sets differ only in the separator thickness, they should both have the same values of b/L_S. We find b/L_S values of (1.42±0.45)×10^{11} s/m^2 and (1.44±0.8)×10^{11} s/m^2 for the L_S=38 and L_S=16 μm separators respectively. Notwithstanding the error, these values are extremely similar as expected from our model. We can also test the absolute values of b/L_S. For the electrolyte and separator used here, we expect σ_{BL}=0.5 S/m and P_S=0.4.[3] Taking the value of b/L_S with the smaller error gives $C_{V,eff}$ =1.8±0.6×10^{10} F/m^3. As mentioned above, a range of electrode materials have shown $C_{V,eff} / Q_V = 28$ F/mAh .[3] Combining the mean low rate specific capacity with the measured average density of these electrodes (3.1 g/cm^3) yields Q_V=6.2×10^8 mAh/m^3, leading to a value of $C_{V,eff} / Q_V = 29$ F/mAh . The similarity of this value to that quoted above shows this NCA *b*-parameter data to be consistent with a range of other electrodes.[3]

We now turn to the *a*-parameter. For the two data sets, these parameters are equal within error (as expected because *a* does not depend on L_S) with a mean value of a=9±1.6×10^{10} s/m^2. Previous work[18] has shown term 1 in equation (2a) can be neglected in most circumstances once σ_{OOP} is above ~0.1 S/m. We measured the mean out-of-plane conductivity of our electrode materials to be σ_{OOP}=0.4 S/m allowing us to remove term 1 from equation (2a). This allows us to write:

$$a \approx \left[\frac{C_{V,eff}}{2\sigma_{BL} P_E^{3/2}} + \frac{1}{D_{BL} P_E^{3/2}} \right]$$

(3b)

Taking the values of $C_{V,eff}$ and σ_{BL} quoted above, calculating P_E=0.31 from the electrode density and taking D_{BL}=3×10^{-10} m^2/s gives a=12±4×10^{10} s/m^2, equal within error to the experimental value.

Finally, we consider the *c*-parameter, which is given by

$$c = \frac{L_S^2}{D_{BL} P_S^{3/2}} + \frac{L_{AM}^2}{D_{AM}} + t_c$$

(3c)

and so describes diffusion within the electrolyte in the separator, solid state diffusion within the active particles as well as the timescale of the electrochemical reaction. Even with the extensive data sets available here, both fits gave values of c to be zero within error. This does not mean that c=0, just that it is too small to be reliably obtained using even these extensive data sets. Using the error margins of the fits, we can obtain an upper bound of c<17 s and c<22 s for the L_S=16 μm and 38 μm data respectively. We can test the validity of this upper limit by considering the three terms in the above equation (i.e. terms 5,6,7 in equation (2a)) individually. Taking D_{BL}=3×10^{-10} m^2/s and P_S=0.4, yields values of 3s and 19s for the first term above for L_S=16 μm and 38 μm respectively. The third term is discussed below but we expect it to be very small. This means that the solid-state diffusion contribution to c is at most 22-19=3 s which limits the possible values of D_{AM}. It has been shown that, for spherical particles of radius, r, the diffusion length $L_{AM}=r/3$.[35] This means that if the solid state diffusion time is <3s, then $D_{AM} > r^2 / 27$. Because the mean radius of primary particles is ~320 nm, this means D_{AM} >4×10^{-15} m^2/s. This is consistent with measurements which show the diffusion coefficient of Li in NCA to be ~10^{-16}-10^{-14} m^2/s (depending on the potential).[36]

Analysis of the exponent, n

Shown in Figure 3C is the exponent n, found by fitting capacity *versus* rate curves, plotted against electrode thickness, L_E, for both separator types. In both cases, n falls very slightly from ~1 at low electrode thickness to ~0.9 for the thicker electrodes. As mentioned above, values of n close to 1 are consistent with electrical (capacitive) effects being rate-limiting while values close to 0.5 indicate diffusive effects to be rate-limiting. With this in mind, the data in Figure 3C would imply thin electrodes to be completely electrically limited while thicker electrodes see a small contribution from diffusive limitations.

We can test this idea by looking at the relative magnitudes of the different terms in equation (2a). In that equation, terms 1, 2, and 4 describe electrical effects while terms 3, 5 and 6 are diffusive in nature (term 7 is the electrochemical reaction time). We can test whether electrical

limitations are indeed dominant by calculating the fraction of τ associated with terms 1, 2 and 4, i.e. τ_E/τ.

In this particular case, this task is simplified by the fact that term 1 is negligible because of the high electrode conductivity while we know from above that c is very small allowing us to neglect terms 5, 6 and 7. This means τ_E/τ is just term 2 + term 4 divided by term 2 + term 3 + term 4. Writing this fraction and rearranging yields:

$$\frac{\tau_E}{\tau} \approx \frac{1+2\dfrac{L_S P_E^{3/2}}{L_E P_S^{3/2}}}{1+2\dfrac{\sigma_{BL}}{C_{V,eff} D_{BL}}+2\dfrac{L_S P_E^{3/2}}{L_E P_S^{3/2}}}$$

(4)

We can plot this fraction in the inset of Figure 3C for each electrode type using the numerical values given above. We find this fraction to approach 1 at low values of L_E, consistent with thin electrodes being purely electrically limited. However, as L_E increases, the fraction falls slightly as diffusive limitations become non-negligible. In addition, the curve for the thin separator is below that of the thicker separator at all electrode thicknesses. All of these properties are consistent with the experimental *n versus* L_E data. This supports our interpretation that the thinnest electrodes are electrically (capacitance) limited with some diffusion limitations appearing as electrodes get thicker. In addition, this analysis shows a degree of consistency between the *n*-data and τ-data, as expressed by equation (2a).

Impedance analysis

While the analysis above shows the values of the *a*- and *b*-parameters to be consistent with the model, it is important to confirm the relatively small values of the *c*-term predicted by the fits in Figure 3B. To achieve this, we performed impedance analysis on all electrodes in order to gather information about t_c as well as to obtain an independent assessment of D_{AM}. The electrodes were evaluated in the charged state (4.3 V) with a 10 mV voltage amplitude using a 1M-0.01 Hz frequency range. Example curves for four different electrode thicknesses are shown in Figure 4 using both linear and logarithmic scales. It is immediately obvious that electrode thickness has a significant effect on the impedance curves. The shapes of the curves

reveal three semi-circles allowing us to propose the equivalent circuit displayed at the top of Figure 4. Using this circuit, we find reasonable fits in all cases.

The impedance fits yield a number of parameters, including four separate resistances, three capacitances (one for each constant phase element) and a Warburg coefficient, all obtained for each value of electrode thickness for two data sets associated with two separator thicknesses. The impedance of a constant phase element is defined as $Z = 1/\left[Q_0 (i\omega)^m \right]$ where Q_0 and m are constants and $0<m<1$. The associated capacitance can be calculated using $C = (Q_0 R_p)^{1/m} / R_p$ where R_p is the parallel resistance in the same circuit element.[37,38] While all parameters are shown in the SI (Figure S5, Table S1), most of them show no significant electrode thickness dependence. However, the resistance, capacitance and Warburg coefficient associated with the rightmost Randles circuit (Figure 4) show large variations with electrode thickness. We associated these parameters with the charge transfer resistance (multiplied by electrode geometric area, A_0), $R_{CT}.A_0$, the double layer capacitance (normalised to A_0), C_{DL}/A_0, and the Warburg coefficient, σ_W. Each of these parameters are plotted versus electrode thickness for both separator types in Figure 5.

We expect the double layer capacitance to scale with the internal surface area associated with the electrode/electrolyte interface. Because thicker electrodes have more internal surface area, this means C_{DL} should scale with electrode thickness. This is shown in figure 5A where we plot C_{DL}/A_0 *versus* L_E. This data shows a linear increase up to L_E~100 μm above which it saturates, falling off at higher thicknesses. We assume such saturation may reflect poor electrolyte penetration at high electrode thickness, consistent with the fall off in low-rate specific capacity shown in Figure 3A.

We can quantitatively analyse the linear increase by noting that the double layer capacitance is given by[39]

$$C_{DL} = \frac{\varepsilon_r \varepsilon_0 A_{Act}}{\lambda} \quad (5a)$$

Where λ is the double layer thickness, ε_0 is the vacuum permittivity, ε_r is the relative permittivity and A_{Act} is the surface area of the electrode/electrolyte interface. Assuming A_{Act} is

the combined surface of all primary particles, then this area is the surface area per particle ($4\pi r^2$) times the number of particles (electrode-mass/mass-per-particle):

$$A_{Act} = \frac{3(1-P_E)A_0 L_E}{r}$$

(5b)

where we use the fact that the ratio of electrode and NCA densities (ρ_E/ρ_{NCA}) can be expressed in terms of the electrode porosity, P_E: $(1-P_E) = \rho_E / \rho_{NCA}$. Combining equations 5a and 5b yields

$$C_{DL} / A_0 = \frac{3\varepsilon_r \varepsilon_0 (1-P_E) L_E}{\lambda r}$$

(5c)

This equation predicts the observed linear increase for thin electrodes. Fitting the low-L_E data and taking[39] λ=1 nm and ε_r=10 yields r=260 nm, close to the mean radius of primary particles as measured by SEM (320 nm). This confirms our association of this capacitance with the double layer.

The linear increase in Figure 5A is consistent with a volumetric double layer capacitance of 0.7 MF/m^3. This is much smaller than the value of $C_{V,eff}$ quoted above which raises questions as to the origin of $C_{V,eff}$ .There is no doubt that battery electrodes have effective capacitances much higher than 0.7 MF/m^3. Typical commercial batteries have capacitances of ~1500 F (18650 cylindrical cell).[40] Assuming the electrodes act like series capacitors, gives a single electrode capacitance of ~3000 F. Approximating the single electrode volume as ~25% of the total yields an electrode volumetric capacitance of ~10^9 Fm^{-3}, in line with $C_{V,eff}$ but much larger than our measured double layer capacitance. Further work is needed to pinpoint the exact origin of $C_{V,eff}$.

The charge transfer resistance is plotted in Figure 5B and falls inversely with electrode thickness, reaching 3×10^{-4} Ω.m^2 for the thickest electrode. We attribute the fall-off with thickness to the fact that the total active nanoparticle surface area increases with electrode thickness. The charge transfer resistance is related to the exchange current density, j_0, via

$R_{CT} = R_G T / n_e F j_0 A_{Act}$,[41] where n_e = 1 is the number of electrons associated with the redox reaction, R_G is the ideal gas constant, T is the temperature and F is the Faraday constant. Using the equation (5b), we obtain:

$$R_{CT} A_0 = \frac{R_G T r}{3 n_e F j_0 (1 - P_E) L_E}$$

(6)

Again, this equation describes the inverse behaviour observed in the graph. Fitting this equation to the data (taking n_e = 1, r = 320 nm, P_E = 31%) yields a value of $j_0 = 4.8 \times 10^{-3}$ mA cm^{-2} of primary particle surface area, somewhat smaller than that previously found from simulations.[42]

The current density crossing the electrolyte-electrode interface can be estimated using the linearized Butler-Volmer equation:[35] $j = j_0 F \eta / R_G T$ where η is the overpotential. We can use this equation to estimate the timescale associated with the electrochemical reaction, t_c (final term in equation (2a)), by linking it to the timescale associated with a charge moving across the interface. Then, $t_c \sim q_A / j$, where q_A is the local charge density per unit area at the electrolyte/NCA interface. This parameter can be estimated from the double layer capacitance $q_A = (C_{DL} / A_{Act}) \Delta V$, where ΔV is the potential drop across the electrolyte/NCA interface. Combining these equations yields: $t_c \sim R_G T (C_{DL} / A_{Act}) \Delta V / j_0 F \eta$. Estimating C_{DL} / A_{Act} ~0.1 F/m^2 from equation (5a) and very crudely taking $\Delta V / \eta \sim 1$ yields t_c~0.05 s. This value is negligible compared to the timescale associated with diffusion through the separator (term 5 in equation 2a) and is certainly consistent with the fits in Figure 3B which show that the c-parameter to be small for both sample sets.

The Warburg coefficient, σ_W, is plotted versus electrode thickness in Figure 5C. Here, we find σ_W to fall inversely with thickness up to L_E~100 μm above which it saturates, again possibly because of poor electrolyte penetration. The Warburg coefficient can be related to the solid-state diffusion coefficient via:[43,44]

$$\sigma_W = \frac{V_M \, | dV / dx |}{F A_{Act} \sqrt{2 D_{AM}}}$$

(7a)

Where V_M=4×10^{-5} m^3/mol is the molar volume of the NCA, and |*dV/dx*| is the magnitude of the rate of change of potential with Li content in the active material (estimated from the GCD curve at the potential where the impedance spectrum was measured, *dV/dx*=-8 V at *V*=4.3 V see Figure S6). We note that A_{Act} is the total interfacial area, as opposed to A_0, the geometric area.[41,45-47] Equation (7a) assumes semi-infinite diffusion and a small voltage perturbation. It is derived for the limiting case where either the perturbation frequency is high, the diffusion coefficient of the species in question is low or for thick electrodes. Our electrodes are significantly thick to satisfy the limiting criteria, which are described in more detail in the work of Ho et al.[44]

Combining equation (7a) and (5b) we find:

$$\sigma_W = \frac{rV_M \,|dV/dx|}{3F(1-P_E)A_0 L_E \sqrt{2D_{AM}}}$$

(7b)

Which gives the inverse dependence on electrode thickness observed in the data. Fitting this curve to the data yields D_{AM}=2×10^{-15} m^2/s at a potential of 4.3V. This value is in agreement with Galvanostatic intermittent titration (GITT) results which yield a diffusivity of ~10^{-15} m^2/s at 4.3 V.[36] In NCA, the diffusion coefficient at 4.3 V is relatively low, with a maximum diffusivity of ~10^{-14} m^2/s expected at 3.8-3.9 V.[36] This means that our D_{AM}-value is consistent with our estimation above that the effective diffusion coefficient is >4×10^{-15} m^2/s.

Taken together, the outputs of the impedance analysis confirm that the *c*-parameter in equation (2b) is small for the electrodes under study here, a result that is consistent with the fitting of the rate data (Figure 3B). Combined with the analysis of the *a*- and *b*-parameters given above, this shows that equation (2a) is in full quantitative agreement with the experimental data. We believe that not only can equation (2a) be used to quantitatively analyse capacity-rate data, but it could even be used to predict the performance of battery electrodes.

We can illustrate the predictive power of our model by using equation (2a), combined with known values of the relevant physical parameters (as quoted in the text above and reproduced in the caption of Figure 6) to plot the predicted L_E-dependence of τ alongside the measured data (Figure 6). For both separators we find an excellent agreement between predicted and measured data, further underlining the validity of equation (2a).

CONCLUSION

In conclusion, we have performed detailed measurements on the effect of electrode thickness on the rate-performance of lithium storing electrodes. We achieved this by using a semi-empirical fitting equation to extract the characteristic time associated with charge/discharge from capacity *versus* rate data for samples with various combinations of electrode and separator thickness. This characteristic time increases super-linearly with electrode thickness. We find that this increase cannot be explained by models based only on liquid phase diffusion. However, the data is completely consistent with a model proposed by us which incorporates various rate-limiting mechanisms including both liquid and solid phase diffusion as well as electrical and electrochemical effects. Fitting the model to the data yields numerical outputs which are (within error) exactly as expected. To support these conclusions, we performed impedance spectroscopy on electrodes with a range of thicknesses. We found significant thickness dependences for the double layer capacitance, the charge transfer resistance and the Warburg coefficient. By combining standard models with a simple equation for the electrolyte-electrode interfacial area, we can fit the thickness-dependent data for each parameter. From these fits, we can show that, for NCA at least, the timescale associated with the electrochemical reaction is small enough not to impact the rate-performance. In addition, we obtain a solid-state diffusion coefficient that is consistent with the outputs obtained by fitting the characteristic time versus electrode thickness data.

METHODS

Electrode Preparation

All electrodes were prepared by the conventional slurry-casting method. $LiNi_{0.815}Co_{0.15}Al_{0.035}O_2$ (NCA, MTI Corp.) powder was mixed with a dispersion of single-walled CNT in N-Methyl-2-pyrrolidone (NMP) (Tuball, 0.4 wt.% CNT in NMP, 2 wt.% Polyvinylidene fluoride (PVDF) as surfactant stabilizer , OCSiAl). The mixture was made uniform using a mortar and pestle. The slurry was then cast onto the Al current collector using a doctor blade. The doctor blade was used to achieve the investigated thickness range (10 – 257 μm, mass loading 3.5 – 75 mg/cm^2). The slurry was then dried overnight at 40 °C. This low temperature is required to avoid cracking in these segregated network composites. We note

that such low temperature drying has been described previously with[6,8] or without[18] an accompanying anneal at 100 °C. Following NMP evaporation, the mass fraction of CNT was 0.5 wt% for all electrodes. Finally, the electrodes were calendered (MSK-HRP-MR100A) to achieve a density of ~3.1 g/cm^3. The morphology of the NCA/CNT electrodes was examined using SEM. An accelerating voltage of 5 keV was used with a 30 μm aperture at a working distance of 5-6 mm (Zeiss Ultra Plus).

Electrochemical Measurements

The electrochemical performance of the electrodes was tested in CR2032 (MTI Corp.) coin-cells. Circular discs (diameter=1.2 cm, A_0=1.13 cm^2) punched from the prepared NCA/CNT films were employed as the working electrode. L_S was varied by using two Celgard separators with different thicknesses, L_S=16 μm (Celgard C212) and L_S=38 μm (Celgard 2340). The electrolyte was 1.2 M $LiPF_6$ in ethylene carbonate/ethyl methyl carbonate (EC/EMC, 1:1 in v/v, BASF) with 10 wt.% fluoroethylene carbonate (FEC). Li metal was used as the counter electrode and the coin-cells were assembled in an Ar-filled glovebox (UNIlab Pro, Mbraun), with O_2 and H_2O levels < 0.1 ppm.

The rate-performance was measured via CA method as we reported previously.[8] The cells were first tested via GCD measurements (BioLogic VMP-3. Three cycles were performed between 3-4.3 V at 1/10 C. After stable capacities were reached (capacity change <1%) and a Coulombic efficiency of >99% was achieved, the cells were charged to the upper cut-off voltage (4.3 V) at 1/10 C. EIS was conducted in a frequency range of 1M-0.01 Hz and with a voltage amplitude of 10 mV (BioLogic VMP-3). EC-Lab's Z Fit software was used to analyse and fit the acquired impedance spectra. Following impedance spectroscopy, the cells were charged to the upper cut-off voltage at 1/30 C (4.3 V) this was done to ensure that the thicker electrodes were fully charged. CA was then performed at the lower cut-off potential (3.0 V).

Current transients from CA were converted to specific capacity (Q/M) vs. rate (R) curves using the following equations: [8,22]

$$\frac{Q}{M} = \int_0^t \left(I/M \right) dt \tag{8a}$$

$$R = \frac{I/M}{Q/M} \quad (8b)$$

where Q is the capacity, M is the active mass, I/M is the specific current and t is the timeframe given by the current transient.

Supporting Information. SEM images, all CA curves, all impedance data, supporting tables.

ACKNOWLEDGEMENTS: We have also received support from the Science Foundation Ireland (SFI) funded centre AMBER (SFI/12/RC/2278_2**),** the European Research Council Advanced Grant (FUTURE-PRINT) and the European Union under grant agreements n°785219 Graphene Flagship-core 2. We also thank Nokia-Bell Labs Ireland for continuing support.

Figures

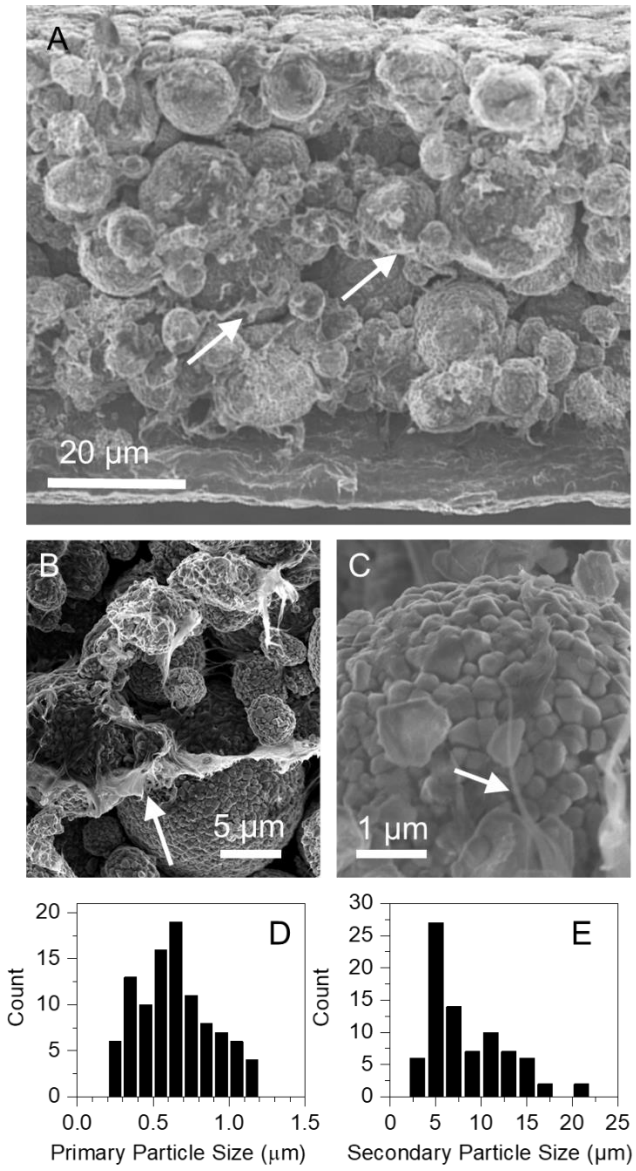

Figure 1: A: Cross-sectional SEM image of a NCA/CNT (0.5 wt.%) segregated network cathode. (B-C): Higher magnification images showing secondary particles and nanotube network (B) as well as the primary particles which make up each secondary particle (C). (D-E): Histograms showing the NCA primary particle length (A) (N = 100) and secondary particle diameter (B) (N = 81). In A-C, the arrows indicate the nanotube networks.

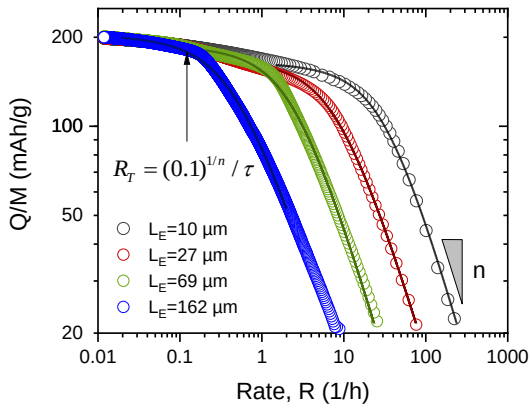

Figure 2: Specific capacity versus rate data plotted for four different electrode thicknesses (L_E), as acquired from chronoamperometry. The curves are fitted to equation (1). The threshold rate, R_T, where the capacity falls below 90% of its low-rate value, is shown for the thickest electrode. In addition, the exponent, *n*, describing the high-rate drop-off in capacity is indicated.

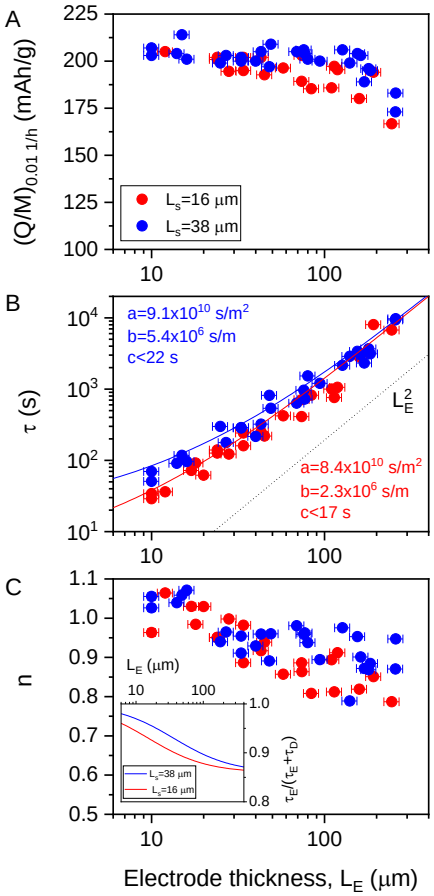

Figure 3: Data extracted from capacity-rate curves shown in Figure 2. A) Experimental specific capacity, measured at 0.01 h^{-1}, $(Q/M)_{0.01\ 1/h}$, plotted as a function of electrode thickness. B-C)

Characteristic time, τ, (B) and rate exponent, n, (C) each plotted versus electrode thickness (L_E). Red and blue data points correspond to a separator thickness, L_S, of 16 and 38 μm, respectively. The fit parameters in B are: L_S=16 μm: a=(8.4±1.7)×10^{10} s/m^2; b=(2.3±1.3)×10^6 s/m; c=2±15 s and L_S=38 μm: a=(9.1±1.6)×10^{10} s/m^2; b=(5.4±1.7)×10^6 s/m; c=0±22 s. The dashed line in B is a plot of $\tau = L_E^2 / D_{BL} P_E^{3/2}$ taking D_{BL}=3×10^{-10} m^2/s and P_E=0.31. Figure 3C, inset: contribution to time constant calculated for electrical effects divided by the sum of contributions due to electrical and diffusive effects. These contributions are calculated using equation (4) as described in the text.

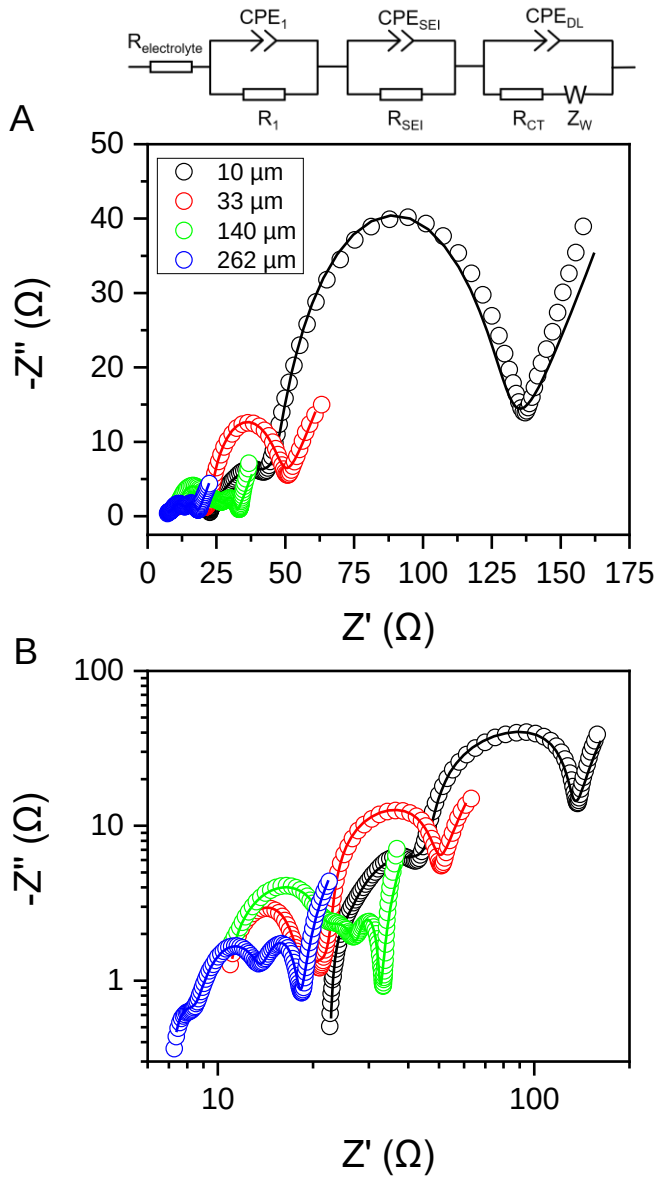

Figure 4: Nyquist plots of imaginary versus real impedance obtained from impedance spectroscopy for four different electrode thicknesses on (A) linear scale and (B) log-log scale. Solid lines represent fits to the circuit shown at the top of the figure.

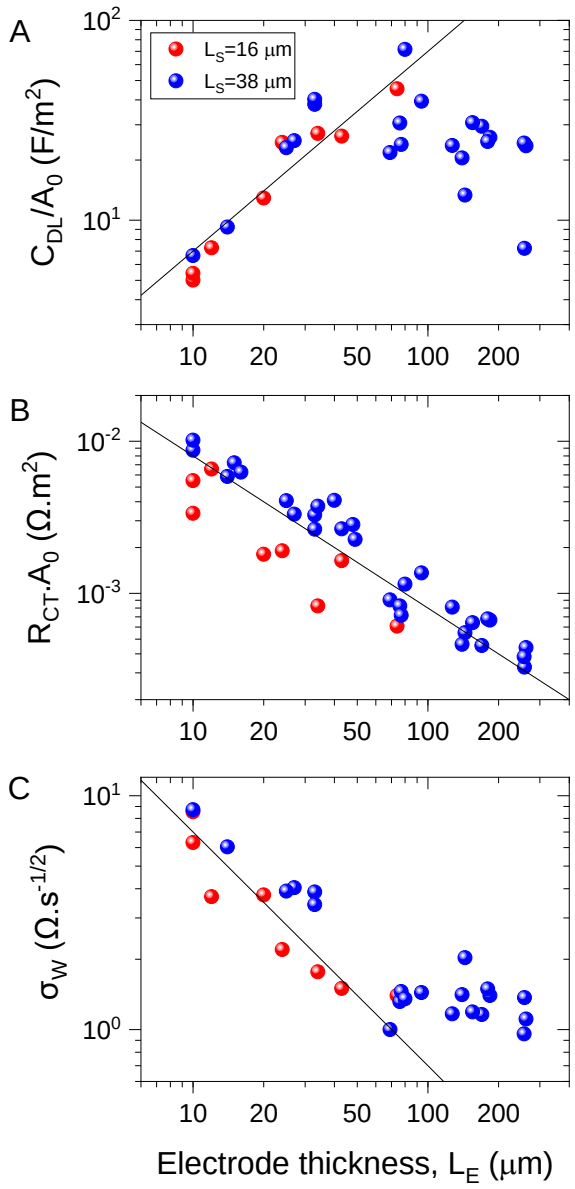

Figure 5: Selected parameters calculated from fitting EIS data, each plotted versus electrode thickness (see SI for all fit parameters). (A) Double-layer capacitance (C_{DL}), (B) Charge-transfer resistance (R_{CT}) and (C) Warburg coefficient (σ_W) versus electrode thickness (L_E). In A and B, the data are adjusted to account for electrode geometric area (A_0). The solid lines indicate fits as described in the text.

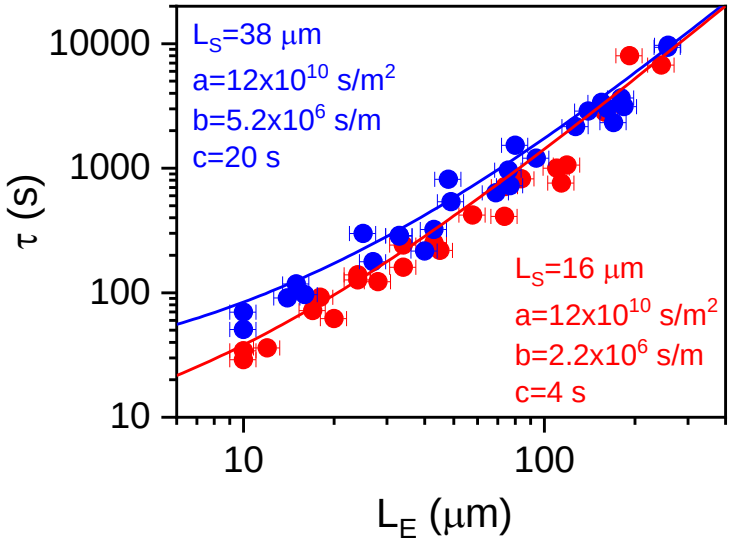

Figure 6: Data for time constant versus electrode thickness for both separator thicknesses. The solid lines represent predictions made using our model by plotting equation (2b) using the parameters given in the panel. These a-, b- and c-parameters were not obtained by fitting but rather were calculated, from equations 3 a,b,c, using known (either independently measured or obtained from the literature) physical parameters. The values of these parameters have been noted in the text i.e. $C_{V,eff} = 28Q_V = 28\times6.2\times10^8$ F/m^3, σ_{BL}=0.5 S/m, P_S=0.4 [see ref [3] for more information about σ_{BL} and P_S], P_E=0.31, $D_{BL}=3\times10^{-10}$ m^2/s, $L_{AM}=r/3$=107 nm, $D_{AM}=10^{-14}$ m^2/s,[36] t_c=0.05 s.

References

1. Scrosati, B.; Garche, J., Lithium Batteries: Status, Prospects and Future. *Journal of Power Sources* **2010,** *195*, 2419-2430.
2. Eftekhari, A., Lithium-Ion Batteries with High Rate Capabilities. *ACS Sustainable Chemistry & Engineering* **2017,** *5*, 2799-2816.
3. Tian, R.; Park, S. H.; King, P. J.; Cunningham, G.; Coelho, J.; Nicolosi, V.; Coleman, J. N., Quantifying the Factors Limiting Rate Performance in Battery Electrodes. *Nature Communications* **2019,** *10*, 1933.
4. Park, S. H.; Tian, R.; Coelho, J.; Nicolosi, V.; Coleman, J. N., Quantifying the Trade-Off between Absolute Capacity and Rate Performance in Battery Electrodes. *Advanced Energy Materials* **2019,** *9*, 1901359.
5. Zheng, H.; Li, J.; Song, X.; Liu, G.; Battaglia, V. S., A Comprehensive Understanding of Electrode Thickness Effects on the Electrochemical Performances of Li-Ion Battery Cathodes. *Electrochimica Acta* **2012,** *71*, 258-265.
6. Park, S.-H.; King, P. J.; Tian, R.; Boland, C. S.; Coelho, J.; Zhang, C.; McBean, P.; McEvoy, N.; Kremer, M. P.; Daly, D.; Coleman, J. N.; Nicolosi, V., High Areal Capacity Battery Electrodes Enabled by Segregated Nanotube Networks. *Nature Energy* **2019,** *4*, 560-567.

7. Heubner, C.; Seeba, J.; Liebmann, T.; Nickol, A.; Börner, S.; Fritsch, M.; Nikolowski, K.; Wolter, M.; Schneider, M.; Michaelis, A., Semi-Empirical Master Curve Concept Describing the Rate Capability of Lithium Insertion Electrodes. *Journal of Power Sources* **2018,** *380,* 83-91.
8. Tian, R.; King, P. J.; Coelho, J.; Park, S.-H.; Horvath, D. V.; Nicolosi, V.; O'Dwyer, C.; Coleman, J. N., Using Chronoamperometry to Rapidly Measure and Quantitatively Analyse Rate-Performance in Battery Electrodes. *Journal of Power Sources* **2020,** *468,* 228220.
9. Choi, J.; Son, B.; Ryou, M. H.; Kim, S. H.; Ko, J. M.; Lee, Y. M., Effect of Licoo2 Cathode Density and Thickness on Electrochemical Performance of Lithium-Ion Batteries. *J. Electrochem. Sci. Technol.* **2013,** *4,* 27-33.
10. Heubner, C.; Nickol, A.; Seeba, J.; Reuber, S.; Junker, N.; Wolter, M.; Schneider, M.; Michaelis, A., Understanding Thickness and Porosity Effects on the Electrochemical Performance of Lini0.6co0.2mn0.2o2-Based Cathodes for High Energy Li-Ion Batteries. *Journal of Power Sources* **2019,** *419,* 119-126.
11. Tian, R.; Breshears, M.; Horvath, D. V.; Coleman, J. N., The Rate Performance of Two-Dimensional Material-Based Battery Electrodes May Not Be as Good as Commonly Believed. *ACS Nano* **2020,** *14,* 3129-3140.
12. Cao, Y. L.; Li, M.; Lu, J.; Liu, J.; Amine, K., Bridging the Academic and Industrial Metrics for Next-Generation Practical Batteries. *Nature Nanotechnology* **2019,** *14,* 200-207.
13. Simon, P.; Gogotsi, Y., Capacitive Energy Storage in Nanostructured Carbon-Electrolyte Systems. *Accounts Chem. Res.* **2013,** *46,* 1094-1103.
14. Heubner, C.; Schneider, M.; Michaelis, A., Diffusion-Limited C-Rate: A Fundamental Principle Quantifying the Intrinsic Limits of Li-Ion Batteries. *Advanced Energy Materials* **2020,** *10,* 1902523.
15. Wong, L. L.; Chen, H. M.; Adams, S., Design of Fast Ion Conducting Cathode Materials for Grid-Scale Sodium-Ion Batteries. *Physical Chemistry Chemical Physics* **2017,** *19,* 7506-7523.
16. Coleman, J. N.; Tian, R., Developing Models to Fit Capacity–Rate Data in Battery Systems. *Current Opinion in Electrochemistry* **2020,** *21,* 1-6.
17. Tian, R.; Alcala, N.; O'Neill, S. J. K.; Horvath, D. V.; Coelho, J.; Griffin, A. J.; Zhang, Y.; Nicolosi, V.; O'Dwyer, C.; Coleman, J. N., Quantifying the Effect of Electronic Conductivity on the Rate Performance of Nanocomposite Battery Electrodes. *ACS Applied Energy Materials* **2020,** *3,* 2966-2974.
18. Tian, R. Y.; Alcala, N.; O'Neill, S. J. K.; Horvath, D. V.; Coelho, J.; Griffin, A. J.; Zhang, Y.; Nicolosi, V.; O'Dwyer, C.; Coleman, J. N., Quantifying the Effect of Electronic Conductivity on the Rate Performance of Nanocomposite Battery Electrodes. *Acs Applied Energy Materials* **2020,** *3,* 2966-2974.
19. Cornut, R.; Lepage, D.; Schougaard, S. B., Interpreting Lithium Batteries Discharge Curves for Easy Identification of the Origin of Performance Limitations. *Electrochimica Acta* **2015,** *162,* 271-274.
20. Johns, P. A.; Roberts, M. R.; Wakizaka, Y.; Sanders, J. H.; Owen, J. R., How the Electrolyte Limits Fast Discharge in Nanostructured Batteries and Supercapacitors. *Electrochemistry Communications* **2009,** *11,* 2089-2092.
21. Gallagher, K. G.; Trask, S. E.; Bauer, C.; Woehrle, T.; Lux, S. F.; Tschech, M.; Lamp, P.; Polzin, B. J.; Ha, S.; Long, B.; Wu, Q. L.; Lu, W. Q.; Dees, D. W.; Jansen, A. N., Optimizing Areal Capacities through Understanding the Limitations of Lithium-Ion Electrodes. *J Electrochem Soc* **2016,** *163,* A138-A149.
22. Heubner, C.; Lämmel, C.; Nickol, A.; Liebmann, T.; Schneider, M.; Michaelis, A., Comparison of Chronoamperometric Response and Rate-Performance of Porous Insertion Electrodes: Towards an Accelerated Rate Capability Test. *Journal of Power Sources* **2018,** *397,* 11-15.
23. Nitta, N.; Wu, F. X.; Lee, J. T.; Yushin, G., Li-Ion Battery Materials: Present and Future. *Materials Today* **2015,** *18,* 252-264.
24. Almar, L.; Joos, J.; Weber, A.; Ivers-Tiffée, E., Microstructural Feature Analysis of Commercial Li-Ion Battery Cathodes by Focused Ion Beam Tomography. *Journal of Power Sources* **2019,** *427,* 1-14.

25. Sironval, V.; Palmai-Pallag, M.; Vanbever, R.; Huaux, F.; Mejia, J.; Lucas, S.; Lison, D.; van den Brule, S., Hif-1α Is a Key Mediator of the Lung Inflammatory Potential of Lithium-Ion Battery Particles. *Particle and Fibre Toxicology* **2019,** *16*, 35.
26. Boland, J. B.; Tian, R.; Harvey, A.; Vega-Mayoral, V.; Griffin, A.; Horvath, D. V.; Gabbett, C.; Breshears, M.; Pepper, J.; Li, Y.; Coleman, J. N., Liquid Phase Exfoliation of Ges Nanosheets in Ambient Conditions for Lithium Ion Battery Applications. *2D Materials* **2020,** *7*, 035015.
27. Vega-Mayoral, V.; Tian, R. Y.; Kelly, A. G.; Griffin, A.; Harvey, A.; Borrelli, M.; Nisi, K.; Backes, C.; Coleman, J. N., Solvent Exfoliation Stabilizes Tis2 Nanosheets against Oxidation, Facilitating Lithium Storage Applications. *Nanoscale* **2019,** *11*, 6206-6216.
28. Zhao, R.; Liu, J.; Gu, J., The Effects of Electrode Thickness on the Electrochemical and Thermal Characteristics of Lithium Ion Battery. *Applied Energy* **2015,** *139*, 220-229.
29. Yu, D. Y. W.; Donoue, K.; Inoue, T.; Fujimoto, M.; Fujitani, S., Effect of Electrode Parameters on Lifepo[Sub 4] Cathodes. *J Electrochem Soc* **2006,** *153*, A835.
30. Zhang, C. F.; Park, S. H.; Ronan, O.; Harvey, A.; Seral-Ascaso, A.; Lin, Z. F.; McEvoy, N.; Boland, C. S.; Berner, N. C.; Duesberg, G. S.; Rozier, P.; Coleman, J. N.; Nicolosi, V., Enabling Flexible Heterostructures for Li-Ion Battery Anodes Based on Nanotube and Liquid-Phase Exfoliated 2d Gallium Chalcogenide Nanosheet Colloidal Solutions. *Small* **2017,** *13*, 1701677
31. Ehrl, A.; Landesfeind, J.; Wall, W. A.; Gasteiger, H. A., Determination of Transport Parameters in Liquid Binary Lithium Ion Battery Electrolytes I. Diffusion Coefficient. *J Electrochem Soc* **2017,** *164*, A826-A836.
32. Ong, M. T.; Verners, O.; Draeger, E. W.; van Duin, A. C. T.; Lordi, V.; Pask, J. E., Lithium Ion Solvation and Diffusion in Bulk Organic Electrolytes from First-Principles and Classical Reactive Molecular Dynamics. *Journal of Physical Chemistry B* **2015,** *119*, 1535-1545.
33. Zhang, B.; Yu, Y.; Liu, Y. S.; Huang, Z. D.; He, Y. B.; Kim, J. K., Percolation Threshold of Graphene Nanosheets as Conductive Additives in Li4ti5o12 Anodes of Li-Ion Batteries. *Nanoscale* **2013,** *5*, 2100-2106.
34. Ye, J. C.; Baumgaertel, A. C.; Wang, Y. M.; Biener, J.; Biener, M. M., Structural Optimization of 3d Porous Electrodes for High-Rate Performance Lithium Ion Batteries. *Acs Nano* **2015,** *9*, 2194-2202.
35. Jiang, F. M.; Peng, P., Elucidating the Performance Limitations of Lithium-Ion Batteries Due to Species and Charge Transport through Five Characteristic Parameters. *Scientific Reports* **2016,** *6*.
36. Dees, D. W.; Kawauchi, S.; Abraham, D. P.; Prakash, J., Analysis of the Galvanostatic Intermittent Titration Technique (Gitt) as Applied to a Lithium-Ion Porous Electrode. *Journal of Power Sources* **2009,** *189*, 263-268.
37. Barsoukov, E.; Macdonald, J. R., *Impedance Spectroscopy: Theory, Experiment, and Applications*. Wiley: 2018.
38. Orazem, M. E.; Tribollet, B., *Electrochemical Impedance Spectroscopy*. Wiley: 2011.
39. Conway, B. E., *Electrochemical Supercapacitors Scientific Fundamentals and Technological Applications*. Springer US: 1999.
40. Zhang, L. J.; Peng, H.; Ning, Z. S.; Mu, Z. Q.; Sun, C. Y., Comparative Research on Rc Equivalent Circuit Models for Lithium-Ion Batteries of Electric Vehicles. *Applied Sciences-Basel* **2017,** *7*, 1002.
41. Bard, A. J.; Faulkner, L. R., *Electrochemical Methods: Fundamentals and Applications*. Wiley: 2000.
42. Dees, D. W.; Gallagher, K. G.; Abraham, D. P.; Jansen, A. N., Electrochemical Modeling the Impedance of a Lithium-Ion Positive Electrode Single Particle. *J Electrochem Soc* **2013,** *160*, A478-A486.
43. Choi, W.; Shin, H.-C.; Kim, J. M.; Choi, J.-Y.; Yoon, W.-S., Modeling and Applications of Electrochemical Impedance Spectroscopy (Eis) for Lithium-Ion Batteries. *J. Electrochem. Sci. Technol* **2020,** *11*, 1-13.
44. Ho, C.; Raistrick, I. D.; Huggins, R. A., Application of Ac Techniques to the Study of Lithium Diffusion in Tungsten Trioxide Thin-Films. *J Electrochem Soc* **1980,** *127*, 343-350.
45. Zhang, J.; Feng, H.; Qin, Q.; Zhang, G.; Cui, Y.; Chai, Z.; Zheng, W., Interior Design of Three-Dimensional Cuo Ordered Architectures with Enhanced Performance for Supercapacitors. *Journal of Materials Chemistry A* **2016,** *4*, 6357-6367.

46. Lvovich, V. F., *Impedance Spectroscopy: Applications to Electrochemical and Dielectric Phenomena*. Wiley: 2015.
47. Winie, T.; Arof, A. K.; Thomas, S., *Polymer Electrolytes: Characterization Techniques and Energy Applications*. Wiley: 2020.

Graphic for manuscript